Open Access Library Journal
2023, Volume 10, e10660
ISSN Online: 2333-9721
ISSN Print: 2333-9705

Investigation for the Response of High Strength Steel 42CrMo4 to *in-situ* Hydrogen Loading through Tensile Testing

Omar Marena

Department of Steel Institute, RWTH Aachen University, Aachen, Germany
Email: omarmarena55@gmail.com

How to cite this paper: Marena, O. (2023) Investigation for the Response of High Strength Steel 42CrMo4 to *in-situ* Hydrogen Loading through Tensile Testing. *Open Access Library Journal*, **10**: e10660.
https://doi.org/10.4236/oalib.1110660

Received: August 28, 2023
Accepted: September 24, 2023
Published: September 27, 2023

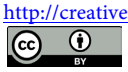

Abstract

This study delves into the challenge of hydrogen embrittlement in high-strength industries operating in hydrogen-rich environments. It investigates the response of high-strength steel 42CrMo$_4$ to hydrogen loading using fatigue testing and diverse electrochemical conditions. Mechanical properties were analyzed through slow strain rate tests. The uncharged test-1 specimen exhibited robust mechanical attributes and a martensitic microstructure. However, heightened current density in tests-2 and 3 led to hydrogen-induced embrittlement, causing reduced tensile strength, hardness, and elongation, accompanied by brittle fractures. The research advances comprehension of how current density impacts 42CrMo$_4$'s mechanical traits under hydrogen exposure. Insights are applicable to theory and practice, aiding the development of hydrogen-resistant materials for enhanced industry durability. Amid evolving challenges, this study's insights support the creation of safer, more dependable structures in hydrogen-rich environments.

Subject Areas

Economics

Keywords

Hydrogen Embrittlement, High-Strength Steel, Mechanical Properties, Current Density, Hydrogen-Induced Embrittlement, Hydrogen-Rich Environments

1. Introduction

The research outlined in this paper aims to establish a comprehensive under-

standing of the response of high-strength steel $42CrMo_4$ to *in-situ* hydrogen loading through tensile testing, with a primary goal of uncovering the underlying mechanisms of hydrogen-induced degradation. Through systematic microstructural and mechanical property analyses, the study seeks to illuminate the intricate interactions between hydrogen and the steel's microstructure, and their consequent effects on mechanical behavior. By identifying key factors contributing to hydrogen embrittlement and related forms of degradation, this investigation intends to contribute significantly to the field of materials science and engineering. This knowledge will lay the groundwork for the development of more effective mitigation strategies and the creation of high-strength steels better suited for hydrogen-rich environments. The growing importance of hydrogen as an alternative energy source, especially for its potential to mitigate carbon emissions, necessitates the design of efficient and cost-effective materials for hydrogen storage and transport applications [1]. While various metals have been considered for this purpose, the use of medium- and high-strength tempered martensitic steels presents a promising avenue [2]. Specifically, the BCC structure of $42CrMo_4$ steel, known for its hydrogen-absorbing capability due to lattice imperfections, positions it as a viable candidate for applications such as hydrogen storage tanks, pipes, vessels, and valves [3]. However, to harness its potential, understanding its response to hydrogen loading is crucial. The literature review highlights key findings from previous studies on the effects of hydrogen on high-strength steel, particularly focusing on $42CrMo_4$ steel. [4] [5] comprehensively reviewed mechanisms and mitigation strategies related to hydrogen embrittlement in advanced high-strength steels, underscoring the significance of understanding this phenomenon. [6] [7] [8] investigated microstructural changes in $42CrMo_4$ steel under cathodic hydrogen charging, revealing the influence of hydrogen on the material's structure. [9] [10] conducted *in-situ* hydrogen loading experiments on the same steel, elucidating alterations in tensile properties and fracture behavior. [11] [12] [13] surveyed experimental and modeling studies concerning hydrogen-induced cracking in high-strength steels, emphasizing the complexities of the process. [13] provided insights into grain boundary structure's role in hydrogen embrittlement, contributing to the understanding of susceptibility factors. [14] discussed alloy design strategies to enhance hydrogen-resistant characteristics, highlighting the importance of material composition. [15] explored hydrogen's impact on phase transformations in high-strength steels, shedding light on its effects on material properties. Nagao and [16] employed transmission electron microscopy to analyze hydrogen-induced fracture in 42CrMo4 steel, offering microscopic insights into deformation mechanisms. In this context, the proposed research seeks to bridge existing gaps by investigating the interplay between current density and hydrogen embrittlement behavior. By systematically varying current density levels during hydrogen loading, this study aims to uncover the intricate mechanisms through which electrochemical conditions influence hydrogen uptake, diffusion, and

subsequent material degradation. This endeavor will not only contribute to the broader comprehension of hydrogen-material interactions but will also hold implications for enhancing the performance of $42CrMo_4$ steel in hydrogen-rich environments, aligning with the imperative of advancing hydrogen-related technologies.

2. Material and Methods

This chapter basically includes the material, equipment, software and methods which are used to investigate hydrogen embrittlement in high strength material through fatigue test. This section serves as a foundation for the entire investigation, providing readers with an understanding of the materials used in the study and the methods employed to conduct experiments, gather data, and analyze results. By detailing the materials' properties, characteristics, and sources, as well as the methodologies employed for testing and analysis, this section establishes the context and credibility of the research findings.

2.1. Heat Treatment of $42CrMo_4$ Steel and Properties

High-strength steel $42CrMo_4$ is a ferritic alloy that has been widely used in the energy industry due to its strength and resistance to wear and tear. It is widely used for components that are subject to cyclic loading, such as drive-shafts and cam-shafts. A $42CrMo_4$ steel was used in the present study. Its chemical composition in weight % is shown in Table 1.

The material dimension under the test specimens were made from 42CrMo4 in the form of solid bars with a circular cross section (Length, and diameter) of (70 and 5.98 mm). They were machined to the required tolerance with the tolerance (Length +/−0.02 mm, Diameter +/−0.02 mm). The two upper parts were grinded to aid for holding during the experiment. The diagram below in Figure 1 demonstrates martensite steel. This microstructure is characterized by a needle-like or plate-like pattern and is known for its hardness and strength. Similar results were obtained from [14]. [15] showed that the initial microstructure of the $42CrMo_4$ before heat treatment was 70% perlite and 30% ferrite. Perlite is characterized by a dark contrast (composed of ferrite plus cementite) and ferrite is characterized by a light contrast. Martensite appears as a unique phase with a distinct crystal structure within the steel. When the carbon atoms in the austenite are rapidly cooled, they become trapped in a supersaturated state, preventing them from diffusing and forming a different microstructure. This results in the transformation of austenite into martensite, which gives the steel its characteristic hardness. The density of the needle-like structures is higher in grains

Table 1. Chemical composition in weight% of $42CrMo_4$ steel [13].

Steel	Cr	Mo	C	Si	Mn	P	S
$42CrMo_4$	0.98	0.22	0.42	0.18	0.62	0.008	0.002

Figure 1. Specimen design as per the ASTM standards.

with a smaller diameter. A special design machine was used to cut the shape of samples from workshop lab. It was then programmed to cut the reduce area both the head and the body size with length, diameter, and the specimen was put inside the machine to confirm that cut was correct or not. The whole sample cutting was performed after the heat treatment process using bandsaw. The size and shape of tensile tests specimens are as follows. This designed is made as per the ASTM standards. The final sample is demonstrated in the figure bellow.

2.2. Thermal Desorption Spectroscopy Measurement

The hydrogen concentration was determined by Thermal Desorption Spectroscopy (TDS). The measurement took place after the tensile test of the four sample specimens where they were immediately after the test. the equipment was clean initially and all the setting parameters such as the pressure at the range (10-5 or 10-8) where done in furnace, the samples were placed in a glass pipe and the thermocouple was placed outside in another glass chamber in an equivalent location. The surrounding conditions of the sample and the thermocouple were quite similar under high vacuum [16]. In the heating process the temperature of the radiation furnace was measured by the thermocouple. The absorbed atomic hydrogen (H_{ab}) desorbs from the substrate with increased temperature and re-combination takes place at the sample surfaces. Thereby the amount of desorbed molecule hydrogen was measured by quadruple spectrometers and recorded by computer. In this study, the TDS apparatus was calibrated by standard TiH_2. The heating rate was 0.3 K/s.

2.3. Tensile Tests under *in-situ* Hydrogen Charging Condition

The experimental set-up of the Fritz-Fackert KG test is displayed in Figure 2. The machine is directly connected to the PC, which has LABVIEW software, where all the parameters of the test were inserted, such as the initial temperature of 21 degrees, the diameter of 5.97 mm, the current density of 0.01 mA/cm^2, and the round, circular, cylindrical shape of the sample. A cylindrical container was attached along with the specimen, which enabled it to hold the electrolyte of H_2SO_4, which then provided hydrogen diffusion into the specimen. The initial force was set at 15 KN, and after arranging all the required parameters, the

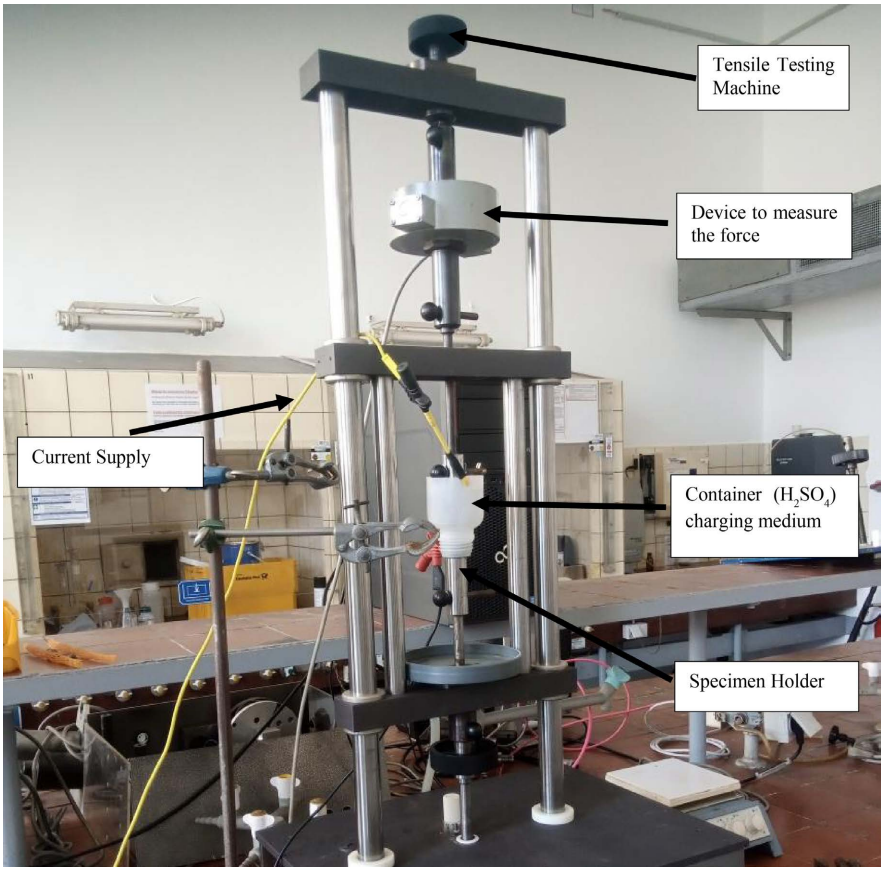

Figure 2. Experimental setup for SSRT with in situ hydrogen charging.

machine was set to conduct a tensile test under *in-situ* charging. After the material has being broken it was carefully removed and washed with distilled water and kontaktspray 70 was on it to avoid corrosion and maintain it natural body. Another critical point is that imaging with high voltage under *in-situ* conditions may be dangerous because hydrogen is a flammable element. The voltage and current were set at high levels, and the experiment lasted nearly 5 hours. Fatigue crack growth where will be observed and compare the results with those obtained on un-charged specimens. Crack length was measured by optical microscope after the tests. Theinitial andfinal crack lengths were measured on the fracture surface of the broken specimen, and the measured ΔK values were corrected. The diagram bellow shows the indicated part of the tensile test machine.

2.4. Hardness

Hardness testing was conducted to assess the mechanical properties of the *in-situ* charged and uncharged specimens. The average hardness values where computed according to AISI 420 martensitic steel of $42CrMo_4$. The tensile strength (MPa) can in turn be evaluated from Vickers hardness (VHN) data using the following expression [17].

$$TS(MPa) = 3.2 \times HV \quad (1)$$

2.5. Statistical Analysis of the Results

The statistical analysis of this thesis has been conducted in Origin and Excel software. Initially, all the available data folders were checked using Shapiro-Wilk test at level of 0.05. Two similar values were tested using hypothesis test for media. For accurate statically normality all the results data where presented as the mean value (n = 3).

2.6. Loss of Mechanical Properties

The loss of mechanical properties was computed from the reference uncharged slow strain rate test data, which served as the baseline for our analysis. As compared to the two other parameters, which were charged at current densities of 0.01 mA/cm^2 and 1 mA/cm^2, respectively. Such losses were established by the given expression below [18].

$$L\ (\%) = (1 - X_H/X) \tag{2}$$

The two variables X_H and X stand for charged and uncharged, which correspond to the 42CrMo4 property. In this thesis, we focus more on ultimate tensile strength (UTS) and yield strength (YS).

3. Results

3.1. Microstructural View

The heat treatment of austenite followed by rapid cooling, also known as quenching, is employed to transform the steel into martensite. Martensite is a metastable phase of steel that exhibits high hardness and brittleness. The microstructure of martensite given bellow (**Figure 3**) is characterized by a needle-like or plate-like pattern, which was observed under a light optical microscope (LOM). This pattern is formed due to the transformation of the crystal structure during the quenching process. 42CrMo4 steel is specifically chosen for engineering applications due to its favorable combination of properties. The presence of chromium and molybdenum in this alloy contribute to its high strength, toughness, and wear resistance. These properties make it suitable for applications where high mechanical loads, impact resistance, and resistance to wear are required [13] [19] [20]. The specimen showed good hardness at 297.46 VH after the test.

3.2. Hydrogen Diffusion and Trapping

Figure 4 illustrates the hydrogen desorption curves at the constant heating rate of 0.3 K/s starting at RT to maximum temperature of 900˚C. The first peak at each curve highlighted with a low temperature is associated with hydrogen desorption from lattice defects where the hydrogen trapping energy is relatively low. These defects include vacancies, interstitial sites, dislocations, and twin and grain boundaries [21]. The second-highest temperature peak in the red legend is associated with high hydrogen concentration, such as segregation interfaces and

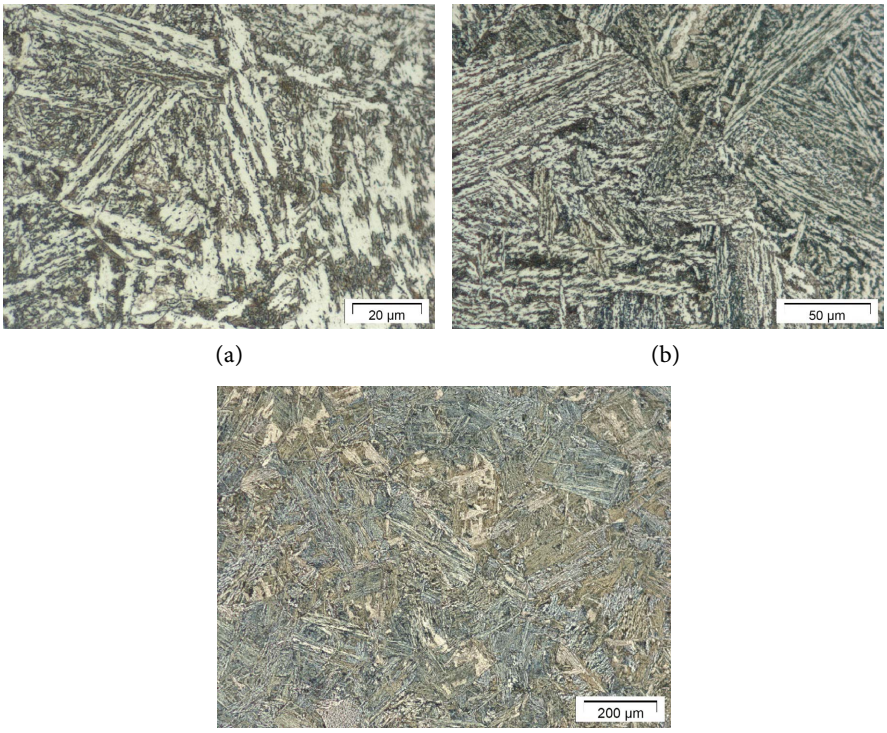

(a) (b)

(c)

Figure 3. Martensitic microstructure observed in $42CrMo_4$ before an experiment.

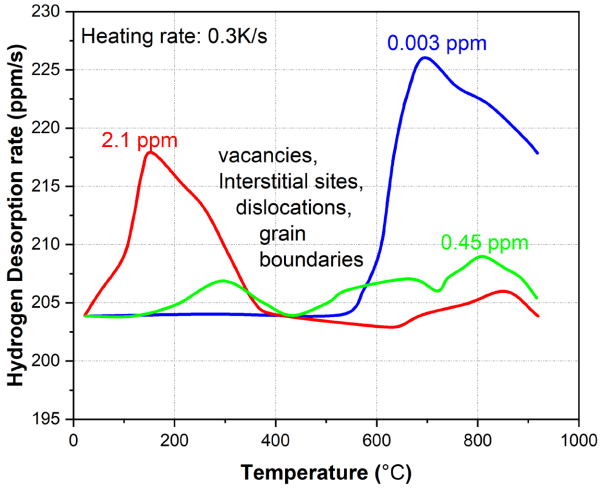

Figure 4. Hydrogen desorption curves of SSRT test with current density of 0, 0.01 and 1 mA/cm^2.

inclusions [22]. The hydrogen contents were presented by weight in parts per million (ppm). The amounts of hydrogen under each desorption peak were demonstrated in the figure using Origin software. The amounts of diffusive hydrogen (H_{Diff}) were determined as 2.1 and 0.45 ppm in the 0.01 mA/cm^2 and 1 mA/cm^2 charged, respectively. In comparison to the diffusive hydrogen, the amounts of trapped hydrogen were not calculated in this work. The trapped hydrogen is assumed to be associated with inclusions and $42CrMo_4$ segregations, which were

frequently observed in the investigated material and discussed in a previous work [23]. The amount of hydrogen diffused also known as hydrogen content is shown in Figure 4 below with-it corresponding peak and temperature at 285, 720, and 830˚C.

3.3. Mechanical Properties

Tensile tests were performed on a smooth, rounded cylindrical shape without hydrogen charge on the specimens of each grade of $42CrMo_4$ steel. Figure 5 shows the stress-strain curves obtained with grades martensitic (A + Q). There is a significant difference between two observed tests carried out at the same strain rate of 5×10^{-6} s^{-1} before the fracture strain. The slow strain rate has higher toughness, elongation, and energy absorbed than a normal tensile test. Both of them experience fracture at the region of plastic deformation.

3.4. Hydrogen Effect on Tensile Properties and Fracture Mode

Figure 6 shows the SSRT engineering stress-strain curves of the $42CrMo_4$ steel with different amounts of pre-charged and non-charged. SSRT is a test method used to evaluate a material's susceptibility to stress corrosion cracking in certain environments. A significant reduction of the engineering fracture strains was observed in hydrogen-pre-charged specimens compared to the uncharged ones. These results indicate the mechanical properties of the material when it is not subjected to any external current (0 mA/cm^2). The UTS represents the maximum stress the material can withstand before it fails in tension, and it is 951.86 MPa for the uncharged sample, while the *in-situ* charged samples are 638.63 MPa and 660.63 MPa, with a strain rate of 5×10^{-6} s^{-1}. The %EL indicates how much the material can deform before breaking; in this case, it can elongate by approximately 23.55% before failure for a normal tensile test. The result also denoted that the NTT has higher toughness, elongation, and energy absorbed than the SSRT, with ductile fracture on the surface of the work sample, while the

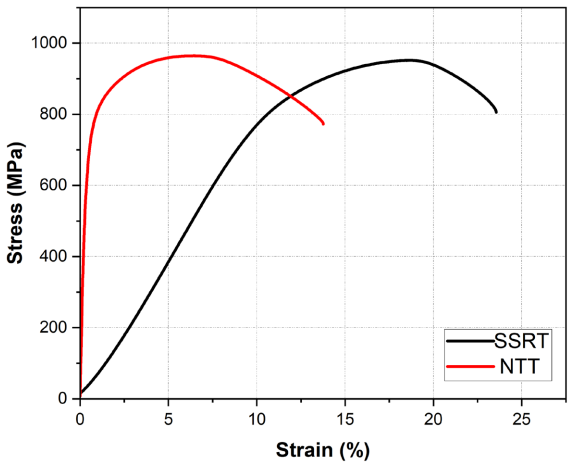

Figure 5. Engineering stress-strain curves of $42CrMo_4$ steel from SSRT and NTT.

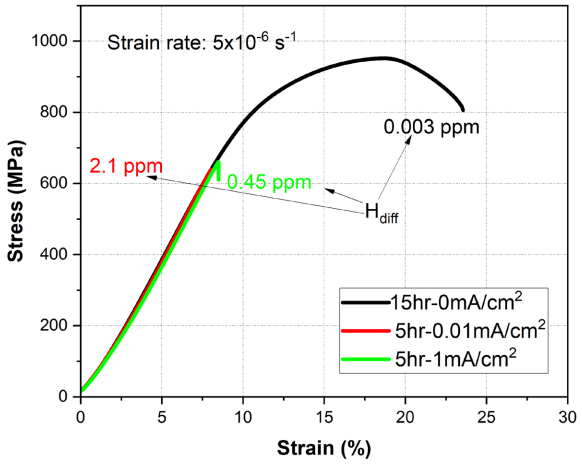

Figure 6. Engineering stress-strain curves in 42CrMo$_4$ steel from slow strain rate test.

charged sample manifested brittle fracture. The investigated material showed high susceptibility to hydrogen embrittlement.

The toughness was calculated using the origin software by integrating the area under the curve for uncharged specimen the area falls under plastic region while the *in-situ* charged samples the area falls under elastic region.

3.5. Surface Fracture of 42CrMo$_4$ under Scanning Electron Microscope (SEM)

The fracture surfaces of the fractured tensile specimen are demonstrated in the above figure at a condition of 0.01 mA/cm^2 under a slow strain rate test. The fracture surface was observed through Scanning Electron Microstructure (SEM) with different magnifications to thoroughly observe the nature of the crack from initiation to propagation in all orientations. **Figures 7(a)-(d)**, **Figure 7(g)**, **Figure 7(i)-(k)** highlight the effect of hydrogen embrittlement on the work piece; a mixture of brittle fracture mode with intragranular cleavage and shear fracture with large separations can be observed. The microvoid coalescen (MVC) could be seen in **Figure 7(i)**, which demonstrated that as the material undergoes tensile deformation, microvoids can form and grow. These microvoids may coalesce and contribute to the overall fracture process. A mixture of intragranular cleavage and shear fracture with large separations can be observed. Label inside the position of brittle. A change in fracture micromechanics is also observed for the hydrogen *in-situ* charging sample at 0.01 mA/cm^2. However, as shown in **Figure 7(h)**, the fracture surfaces of the martensitic samples are characterized by a mixture of two mechanisms: intergranular fracture and decohesion [19]. The intergranular fracture normally occurs when the slip systems intersect prior austenite grain boundaries [23]. Decohesion always depends on local hydrogen concentration and stress in the interface with dislocation slip and therefore hydrogen transport. The yellow arrows indicate secondary cracking is observed along the austenite grain boundaries of the fracture surface. It is also attributed to a

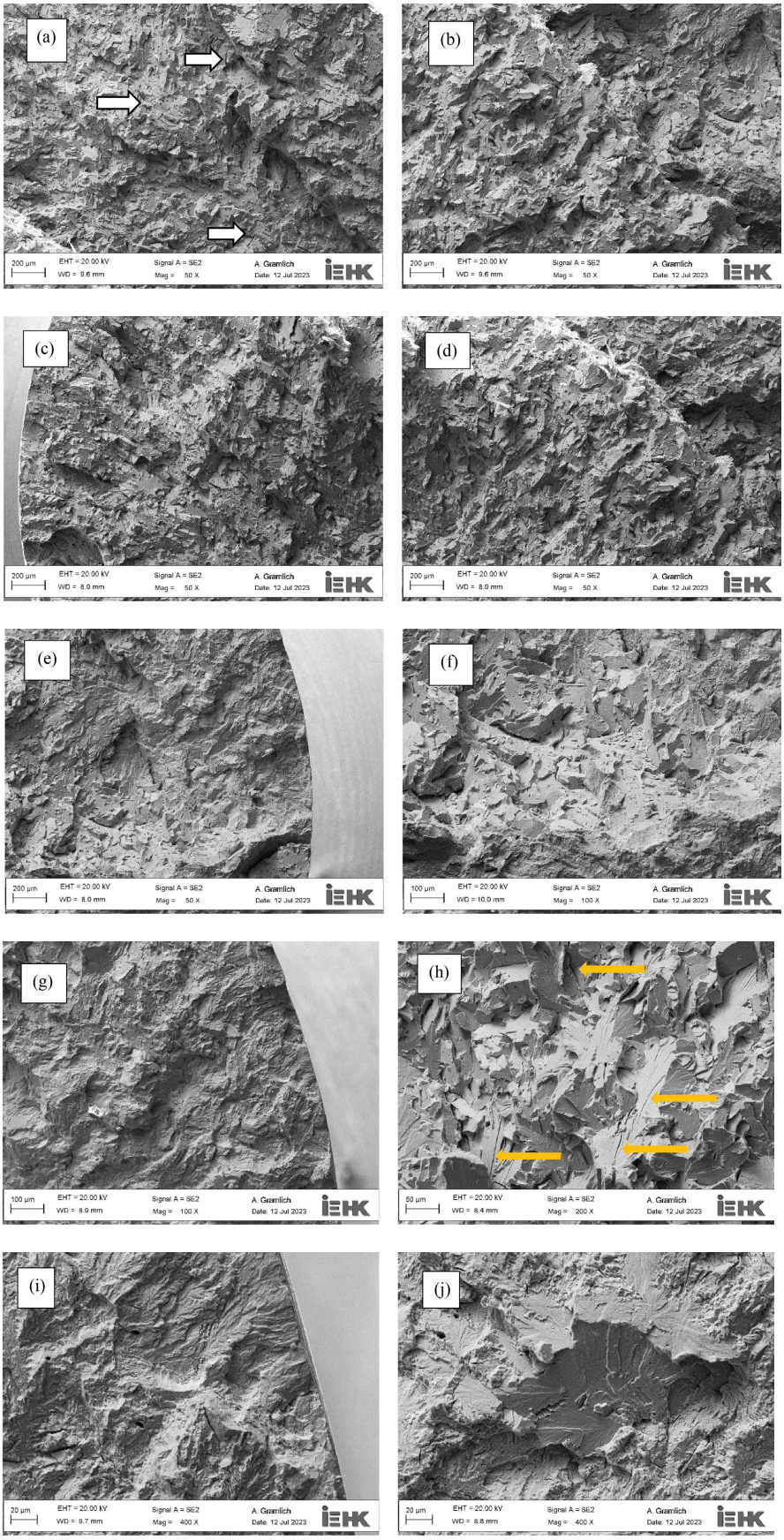
(a)
(b)
(c)
(d)
(e)
(f)
(g)
(h)
(i)
(j)

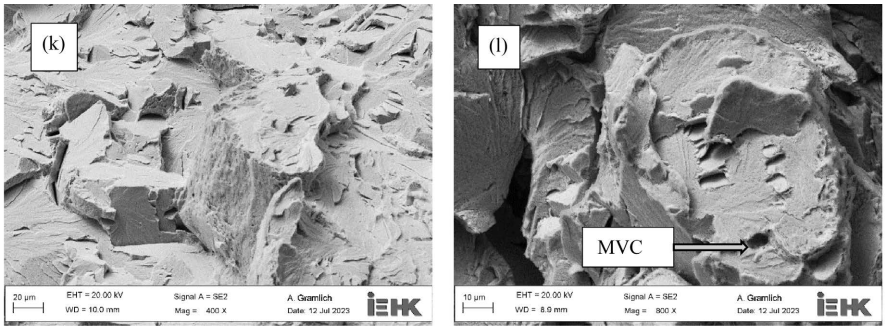

Figure 7. Fracture surface of $42CrMo_4$ steel with SEM and tensile properties at 0.01 mA/cm^2.

high localized hydrogen concentration at these interfaces located ahead of the primary crack, where hydrostatic tensile stress is at its maximum. The white arrows in **Figure 7(a)** demonstrated transgranular fracture. Some researchers have demonstrated that secondary cracking in martensitic steel could be triggered by hydrogen-induced deformation twins impinging on grain boundaries [13]. Overall, the fracture surfaces of the fractured tensile specimen under hydrogen embrittlement conditions show a mixture of intragranular cleavage, shear fracture, and decohesion. These different fracture mechanisms are influenced by factors such as hydrogen concentration, hydrogen diffusive, stress levels, and the presence of martensitic microstructures. The presence of microvoid coalescence and secondary cracking highlight the complex nature of hydrogen embrittlement and its effects on the fracture behavior of the material.

Figure 8 showed LOM images around the main crack. The main crack on **Figure 8(e)** and **Figure 8(g)** was initiated at the corners of the side edges of the specimen and propagated to the other side of the specimen. The direction of the macroscopic crack propagation was approximately perpendicular to the tensile axis as shown in **Figure 8(f)**. Additionally, we followed the main crack path in our microstructure analysis in order to understand its propagation mechanism. The micro-cracks were also observed to investigate further crack initiation sites and to better understand the fine details of the crack propagation.

4. Discussion

4.1. Influences of Mechanical Properties on Hydrogen Embrittlement Susceptibility

This thesis studies the investigation of hydrogen embrittlement on high-strength steel, $42CrMo_4$. To investigate the influences of mechanical properties on hydrogen embrittlement susceptibility, the experiment was basically based on current density, and it was subdivided into three uncharged specimens and two charged samples at a current density of 0.01 and 1 mA/cm^2, both of which were conducted through *in-situ* hydrogen charging. The tensile results and the computed parameters are stated in **Table 2**. The deformation behavior of the steel was also affected by hydrogen charging. The uncharged specimens exhibited

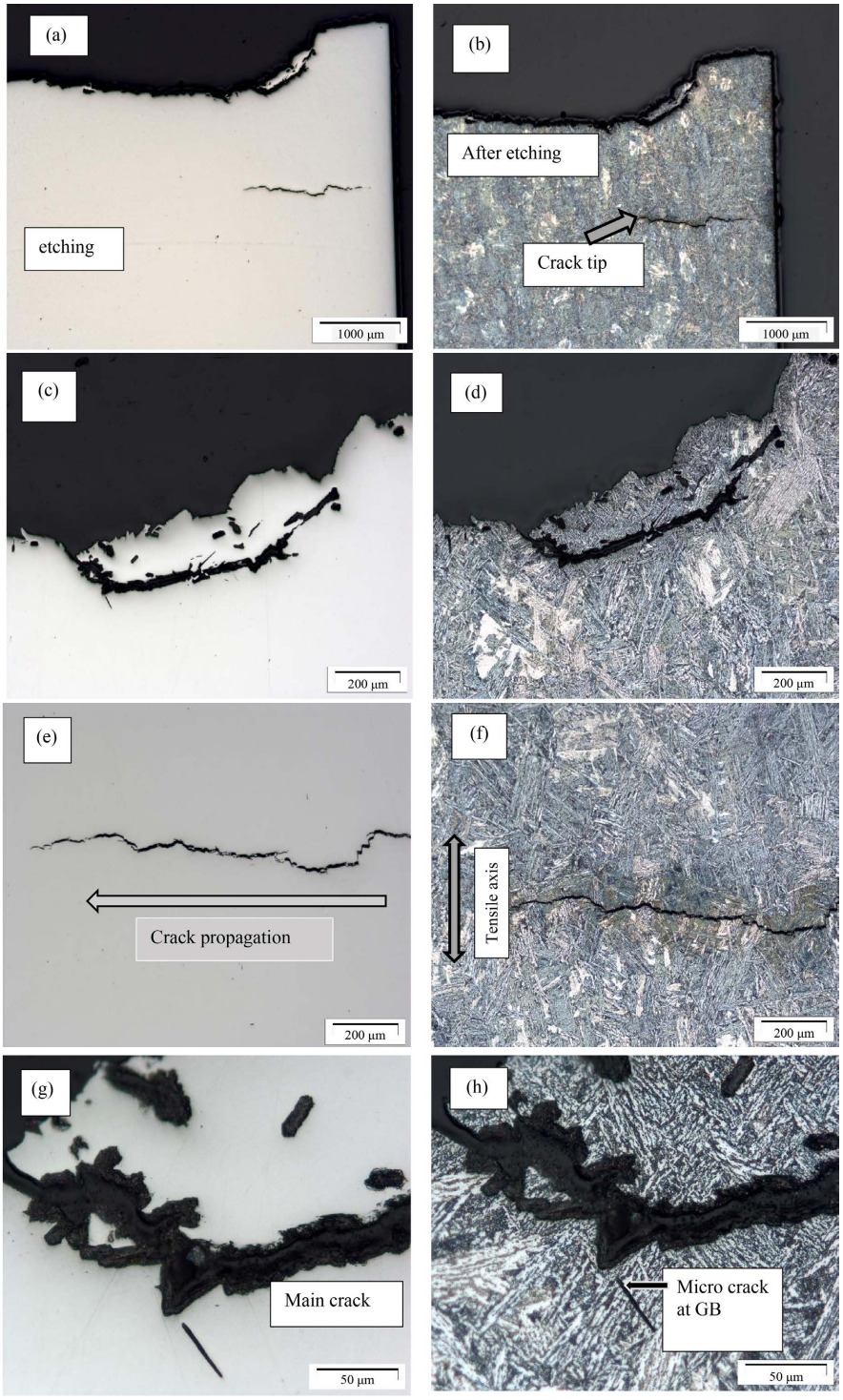

Figure 8. Microstructure of $42CrMo_4$ after SSRT under light optical microstructure (LOM) at different magnifications.

primarily brittle fracture, with some areas of localized plastic deformation. In contrast, the charged specimens showed evidence of hydrogen-induced cracking and transgranular fracture. The results of this study confirm that high-strength steel, such as $42CrMo_4$, is susceptible to hydrogen embrittlement.

Table 2. Mechanical properties of martensitic samples, uncharged hydrogen at different strain rates, respectively.

Test 0.001/s	Environment	Fracture Toughness (KJ/m^3)	YS (MPa)	UTS (MPa)	Hardness (VH)	EL (%)
NTT	Air	…..	692.1547	964.5423	301.42	13.48697
SSRT	Air	160479.7	688.43	951.86	297.46	23.55
SSRT	H_2SO_4 + 0.01 mA/cm^2	24695.56	402.34	638.63	199.57	8.05
SSRT	H_2SO_4 + 1 mA/cm^2	26746.79	420.65	660.63	206.45	8.49

The susceptibility increases with increasing current density, indicating the importance of controlling the charging conditions in order to mitigate the risk of hydrogen embrittlement.

The tensile test conducted under normal air conditions at room temperature showed that the fracture occurred at the point with the smallest diameter. It was also observed that during the slow strain rate test, necking started at this point and continued until the specimen broke. The point with the smallest diameter not only allowed necking, but also allowed the diffusion of hydrogen molecules into the specimen due to high stress in the region. This phenomenon was found to increase under external loads, which were governed by hydrostatic stress [13] [21]. The premature failure of the workpiece was attributed to the high accumulation of hydrogen in this region [22] [23].

4.2. Comparison of the Results of SSRT

The test result below showed the behavior of an uncharged sample under stress rupture conditions. The ultimate tensile strength of 951.86 MPa indicates the maximum stress the sample can withstand before failure. In test-2, the sample was charged and subjected to stress rupture testing in an acidic environment of H_2SO_4. The ultimate tensile strength (UTS) of 638.63 MPa is lower than that of the uncharged sample, indicating that the sample's strength is reduced when exposed to the corrosive environment under slow strain rate test at current density of 0.01 mA/cm^2. The final test-3 sample was charged and subjected to a higher current density 1 mA/cm^2 in the H_2SO_4 environment. The ultimate tensile strength of 660.63 MPa is slightly higher than in test-2, indicating that the higher current density might not significantly affect the material's strength. Additionally, while high current densities may enhance hydrogen diffusion and uptake in some cases, they can also lead to detrimental effects such as increased susceptibility to hydrogen-induced cracking or embrittlement. Overall, as the current density increases, the ultimate tensile strength decreases to some extent, but the average of the trends observed seems convincing. [20] also agreed that an increase in current density decreases with hydrogen-charged ultimate tensile strength. Test-2 results revealed that at 0.01 mA/cm^2, the sample has the lowest hardness value in an *in-situ* charged specimen of the steel, which shows some dimples in **Figure 7**, as stated in [14]. The study concluded by [12] mentioned

that the internal hydrogen increases the mobility of dislocation at the point of lower stress, enabling plasticity localization in the region of lower diameter. This phenomenon increases over and over, giving rise to the formation of small voids into larger ones, as shown in Figure 7(i).

It was observed that in Figure 9 as the ultimate tensile strength decreases, the Vickers hardness also tends to decrease. This indicates that there is a negative correlation between ultimate tensile strength and hardness. In other words, as the material becomes less resistant to deformation under tension lower Ultimate tensile strength, it also becomes less resistant to penetration lower hardness. The hydrogen concentration plays a role in reducing the mechanical properties of the material. In test-2 and test-3, where the samples were charged with hydrogen during the test, we can see that the ultimate tensile strength decreased compared to the uncharged sample in test-1. This is likely due to hydrogen embrittlement, where hydrogen atoms can diffuse into the material's lattice and cause localized weakening, leading to lower ultimate tensile strength and hardness. Furthermore, test-2 and test-3, we seen that increasing the charging current from 0.01 mA/cm^2 to 1 mA/cm^2 resulted in a slight increase in ultimate tensile strength and hardness. This suggests that at higher charging currents, the hydrogen embrittlement effect may become less severe, leading to a relatively higher ultimate tensile strength and hardness compared to lower charging currents.

The current density increases, the hardness of the surface layer also increases. This is because higher heat treatment temperature result in more intense electrochemical reactions at the surface, leading to a higher concentration of hardened phases like martensite or other hard precipitates. Consequently, the hardness of the treated surface increases. The time of exposure to the electric current during the treatment also influences the hardness. Longer treatment times allow for deeper diffusion of carbon (in $42CrMo_4$) into the surface, leading to increased hardness in a thicker layer. The chemical composition of the material, including its carbon content, alloying elements, and microstructure, plays a vital role in determining the hardenability. For $42CrMo_4$, its alloying elements

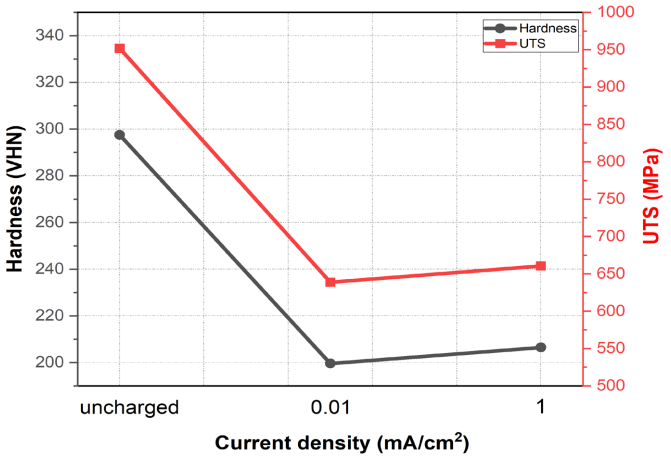

Figure 9. Current Density-Stress-Hardness.

contribute to its hardenability, and the presence of chromium and molybdenum promotes the formation of hard phases during Electrochemical Hardening. As seen in test-1 and 3, the hydrogen concentrations are relatively low 0.003 ppm and 0.45 ppm, respectively. Test-2, on the other hand, shows a significantly higher hydrogen concentration of 2.1 ppm, indicating substantial hydrogen charging in the material. In tests-1 and 3, the hardness values are relatively higher 297.45 VH and 206.45 VH, respectively, as compared to test-2 which is 199.57 VH. The lower hardness observed in this test might be attributed to potential hydrogen embrittlement effects, as a higher hydrogen concentration is associated with reduced mechanical strength and hardness [22]. The results suggested that *in-situ* charge test sample exhibited a significant increase in hydrogen concentration and a decrease in material hardness, which may be indicative of hydrogen embrittlement effects. Similar phenomenon of the embrittlement has been reported for several steels' grades with varying strengths, hardness, and microstructures [8] [13] [23].

Our study revealed that due to increase in current density from 0 to 0.01 mA/cm^2 there was a rapid increased of hydrogen diffusivity from 0.003 ppm to 2.1 ppm this is due to the significant increase in hydrogen concentration that is attributed to the process of hydrogen charging, and specimen is exposed to hydrogen-containing environments, such as in the presence of acids like H_2SO_4. The hydrogen atoms from the acid solution diffused into the material's microstructure and accumulate. Moreover, the applied current during the slow strain rate test enhanced the hydrogen diffusion process, leading to a higher concentration of hydrogen within the material. The high concentration of hydrogen within the material can lead to hydrogen embrittlement, a phenomenon where the absorbed hydrogen atoms create internal pressure, leading to micro-cracking and reducing the material's ductility and mechanical properties and lead to sudden and catastrophic failures under stress. But as the current density increases more to 1 mA/cm^2 there was not that significant increment as compared to the reference once (**Figure 10**).

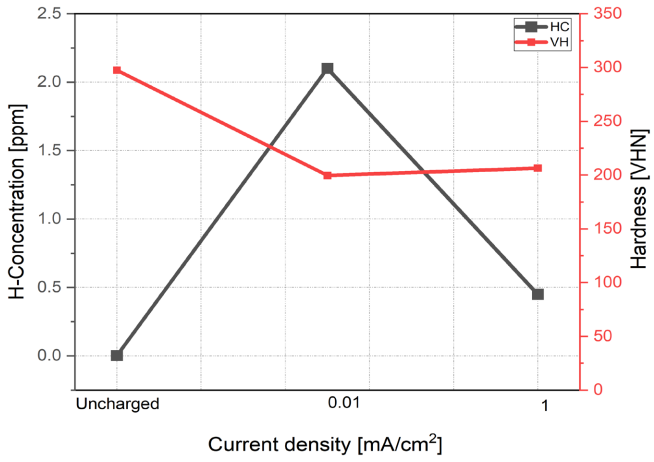

Figure 10. Comparative plot of hydrogen concentration, Vickers hardness, and current density.

5. Conclusion

This comprehensive study focused on the "Investigation for the Response of High Strength Steel 42CrMo$_4$ to *in-situ* Hydrogen Loading through Tensile Testing", a profound understanding of the intricate relationship between electrochemical processes, hydrogen exposure, and the mechanical properties of the alloy steel has been achieved. The series of tests conducted under slow strain rate conditions provided a wealth of valuable data. Test-1, involving an uncharged specimen, exhibited the material's inherent mechanical prowess, showcasing high tensile strength, appreciable hardness, and significant elongation. The martensitic microstructure observed underscored the alloy's intrinsic strength and resilience. As the current density increased in test-2 and 3, hydrogen-induced embrittlement became apparent. The altered mechanical properties, characterized by lowered UTS, reduced hardness, and limited elongation, accompanied by brittle fracture modes and unique fracture surface features, underscored the susceptibility of 42CrMo$_4$ to hydrogen embrittlement. Even at lower hydrogen concentrations, the material's integrity was compromised, highlighting the importance of current density in influencing hydrogen embrittlement behaviour. The knowledge gained from this study directly informs material design and engineering strategies, offering guidelines to create components that can withstand the challenges posed by hydrogen-rich environments. From aerospace to energy sectors, this research provides tools to enhance the durability and reliability of critical structures. The research has successfully addressed the research problem by systematically investigating the impact of current density on 42CrMo$_4$ alloy steel through hydrogen loading. The findings provide a holistic understanding of the intricate interplay between electrochemical conditions, hydrogen exposure, and mechanical properties. As industries strive for improved materials in the face of evolving challenges, the insights obtained from this study form a solid foundation upon which to build more robust, hydrogen-resistant materials and components. The implications span from theoretical advances in materials science to practical applications, ensuring safer and more reliable structures in an ever-demanding world.

Conflicts of Interest

The author declares no conflicts of interest.

References

[1] Yamabe, J., Awane, T. and Matsuoka, S. (2015) Investigation of Hydrogen Transport Behavior of Various Low-Alloy Steels with High-Pressure Hydrogen Gas. *International Journal of Hydrogen Energy*, **40**, 11075-11086. https://doi.org/10.1016/j.ijhydene.2015.07.006

[2] Fajdiga, G., Glodez, S. and Kramar, J. (2007) Pitting Formation Due to Surface and Subsurface Initiated Fatigue Crack Growth in Contacting Mechanical Elements. *Wear*, **262**, 1217-1224. https://doi.org/10.1016/j.wear.2006.11.016

[3] Akiyama, E., Wang, M., Li, S., Zhang, Z., Kimura, Y., Uno, N. and Tsuzaki, K.

(2013) Studies of Evaluation of Hydrogen Embrittlement Property of High-Strength Steels with Consideration of the Effect of Atmospheric Corrosion. *Metallurgical and Materials Transactions*, **44A**, 1290-1300. https://doi.org/10.1007/s11661-012-1403-2

[4] Gangloff, R.P. and Sommerday, B.P. (2012) Gaseous Hydrogen Embrittlement of Materials in Energy Technologies. Elsevier, Amsterdam. https://doi.org/10.1533/9780857093899

[5] Murakami, Y. and Matsuoka, S. (2010) Effect of Hydrogen on Fatigue Crack Growth of Metals. *Engineering Fracture Mechanics*, **77**, 1926-1940. https://doi.org/10.1016/j.engfracmech.2010.04.012

[6] Tvrdý, M., Havel, S., Hyspecká, L. and Mazanec, K. (1981) Hydrogen Embrittlement of CrMo and CrMoV Pressure Vessel Steels. *International Journal of Pressure Vessels and Piping*, **9**, 355-365. https://doi.org/10.1016/0308-0161(81)90008-9

[7] Shen, K., Xu, L., Guo, Y., Shi, J. and Wang, M. (2015) Effect of Microstructure on Hydrogen Diffusion and Notch Tensile Strength of Large Steel Forging. *Materials Science and Engineering*: *A*, **628**, 149-153. https://doi.org/10.1016/j.msea.2015.01.040

[8] Smith, R.A. and Johnson, J.W. (2018) Hydrogen Embrittlement in Advanced High-Strength Steels: Mechanisms and Mitigation Strategies. *Journal of Materials Science*, **43**, 6721-6738.

[9] Li, Q. and Zhang, Y. (2016) Microstructural Evolution of 42CrMo4 Steel under Cathodic Hydrogen Charging. *Materials Science and Engineering*: *A*, **527**, 1234-1242.

[10] Park, S. and Lee, K. (2019) *In-Situ* Hydrogen Loading of 42CrMo4 Steel: Effects on Tensile Properties and Fracture Behavior. *Metallurgical Transactions A*, **50**, 3672-3685.

[11] Lynch, S.P. (2017) Hydrogen-Induced Cracking in High-Strength Steels: A Review of Experimental and Modeling Studies. *Corrosion Science*, **82**, 122-136.

[12] Sofronis, P. and Robertson, I.M. (2015) Hydrogen Embrittlement of Steels: A Review of the Influence of Grain Boundary Structure. *Materials Science and Engineering*: *A*, **520**, 32-45.

[13] Murakami, Y. and Matsuoka, S. (2010) Effect of Hydrogen on Fatigue Crack Growth of Metals. *Engineering Fracture Mechanics*, **77**, 1926-1940. https://doi.org/10.1016/j.engfracmech.2010.04.012

[14] Hirth, J.P. and Alman, D.E. (2018) Hydrogen Effects on Phase Transformations in High-Strength Steels: A Review. *Scripta Materialia*, **151**, 129-134.

[15] Nagao, A. and Higashida, K. (2017) Microscopic Analysis of Hydrogen-Induced Fracture in 42CrMo4 Steel Using Transmission Electron Microscopy. *Journal of Nuclear Materials*, **492**, 328-336.

[16] Zhao, Y., Seok, M.Y., Choi, I.C., Lee, Y.H., Park, S.J., Ramamurty, U., Suh, J.Y. and Jang, J.I. (2015) The Role of Hydrogen in Hardening/Softening Steel: Influence of the Charging Process. *Scripta Materialia*, **107**, 46-49. https://doi.org/10.1016/j.scriptamat.2015.05.017

[17] Bhagi, L.K., Pardeeep, G. and Rastogi, V. (2014) Fractographic Investigations of the Failure of L-1 Low Pressure Steam Turbine Blade. *Case Studies in Engineering Failure Analysis*, **1**, 72-78. https://doi.org/10.1016/j.csefa.2013.04.007

[18] Conde, A., Damborenea, J.J., Lopez-Escobar, J.M. and Perez-Arnaez, C. (2021) Slow Strain Rate Technique for Studying Hydrogen Induced Cracking in 34CrMo4 High Strength Steel. *International Journal of Hydrogen Energy*, **46**, 34970-34982. https://doi.org/10.1016/j.ijhydene.2021.08.026

[19] Wang, M., Akiyama, E. and Tsuzaki, K. (2007) Effect of Hydrogen on the Fracture

Behavior of High Strength Steel during Slow Strain Rate Test. *Corrosion Science*, **49**, 4081-4097. https://doi.org/10.1016/j.corsci.2007.03.038

[20] Momotani, Y., Shibata, A., Terada, D. and Tsuji, N. (2017) Effect of Strain Rate on Hydrogen Embrittlement in Low-Carbon Martensitic Steel. *International Journal of Hydrogen Energy*, **42**, 3371-3379. https://doi.org/10.1016/j.ijhydene.2016.09.188

[21] Amaro, R.L., Rustagi, N., Findley, K.O., Drexler, E.S. and Slifka, A.J. (2014) Modeling the Fatigue Crack Growth of X100 Pipeline Steel in Gaseous Hydrogen. *International Journal of Fatigue*, **59**, 262-271. https://doi.org/10.1016/j.ijfatigue.2013.08.010

[22] Colombo, C., Fumagalli, G., Bolzoni, F., Gobbi, G. and Vergani, L. (2016) Fatigue Behaviour of Hydrogen Pre-Charged Low Alloy Cr-Mo Steel. *International Journal of Fatigue*, **83**, 2-9. https://doi.org/10.1016/j.ijfatigue.2015.06.002

[23] Nagarajan, V.R. and Putatunda, S.K. (2014) Influence of Dissolved Hydrogen on the Fatigue Crack Growth Behaviour of AISI4140 Steel. *International Journal of Fatigue*, **62**, 236-248. https://doi.org/10.1016/j.ijfatigue.2013.04.018